INCREASING THE NRI BANDWIDTH OF DIELECTRIC SPHERE-BASED METAMATERIALS BY COATING

S. Yan[*] and G. A. E. Vandenbosch

ESAT-TELEMIC, Katholieke Universiteit Leuven (KUL), Kasteelpark Arenberg 10 bus 2444, B-3001 Leuven, Belgium

Abstract—A new metamaterial topology is proposed, based on dielectric coated spheres. The effect of the coating is an increased negative permittivity and permeability bandwidth compared with the non-coated spheres. The influence of the dimensional parameters is analyzed, and the relation of each of them with the bandwidth is studied. The theoretical results are confirmed by full wave simulations using CST. A combination of the new topology with wires is used to reach an NRI bandwidth of about 23%. To the knowledge of the authors, to date this is one of the highest bandwidths reported in literature.

1. INTRODUCTION

Metamaterial (MMs) have attracted much attention in the recent decade, mainly for their unique properties and potential applications, since they allow engineers to synthesize artificial materials according to their own needs. A large class of MMs displays a negative refractive index (NRI), i.e., their permittivity and permeability are negative simultaneously. As early as 1968 [1], Veselago theoretically investigated NRI MMs, and predicated some strange electromagnetic effects in these media. After that, MMs disappeared from literature for about 30 years, until Pendry used an array of split ring resonators (SRR) and metallic wires to build a real medium that exhibits the NRI properties in the microwave band [2]. After that, the interest in this field resurged. Huge numbers of scientists studied similar structures, like the double SRR [3], single SRR [4], omega-shaped structures [5], S-shaped [6] and U-shaped structures [7], and spiral resonators [1, 8]. Though all of these have different metallic structures and performances, the basic principle

* Corresponding author: Sen Yan (sen.yan@esat.kuleuven.be).

is nearly the same. The unit cell resonates at a certain frequency, whose wavelength is much larger than the size of the cell. Both theory and experiments have shown that the result is significant. However, a series of inherent defects are exhibited, like anisotropy, conductor loss, narrow bandwidth, and also a difficult fabrication in the optical band.

Another route based on Mie resonances of dielectric particles was proposed to solve the above problems. Gans and Happel were the first ones to investigate a dielectric sphere array more than 100 years ago [9]. Within the context of metamaterials, in 2003, Holloway et al. pointed out that small spheres with large permittivity and permeability could give an effective negative permittivity and negative permeability [10]. They used Lewin's formula [11] to calculate the effective properties of the mixture. After that in 2004, Vendik and Gashinova [12] used spheres with only large permittivity but different sizes to realize the NRI. The authors claimed that this is much easier to fabricate in practice. In 2006, Jylhä et al. [13] established a theoretical model using the Clausius-Mossotti relation [14], which is more accurate than Lewin's model. Wheeler et al. (2006) [15] and Basilio et al. (2012) [16] simplified things and used spheres of the same size only to realize NRI. Kuester et al. [17] obtained an NRI bandwidth of ca. 10% by using layered dielectric spheres while considering realistic losses. Experiments on single sphere structures were performed only by Peng et al. (2007) [18], Zhao et al. (2008) [19], Cai et al. (2008) [20], and Lepetit et al. (2009) [21]. Several kinds of all-dielectric MMs were fabricated and tested to verify the NRI characteristics. Liu et al. derived an effective circuit model for this structure in 2011 [22]. This model is more intuitive and gives an analytical dependency on the electromagnetic and geometrical parameters of the composite. Yannopapas and Moroz (2005) [23] and Garcia-Etxarri et al. (2011) [24] used the dielectric sphere structure to obtain the NRI phenomenon at terahertz and infrared frequencies, respectively.

All-dielectric MMs certainly have no conductor losses, and are quasi-isotropic due to inherent symmetries. However, their bandwidth is still a difficult problem. A higher packing density can give a stronger coupling, which means more bandwidth (Ahmadi and Mosallaei 2007 [25] and Vendik et al. 2009 [26]). The highest packing density is limited by the size of the particles and the space between them.

In order to extend the NRI bandwidth considerably, in this paper, an alternative method is proposed and theoretically investigated. The technique involves changing the particles themselves by coating them. Coating the spheres generates more degrees of freedom to control the resonance. After this introduction, in the second section, the existing

model for all-dielectric single spheres is used, to the knowledge of the authors for the first time, to study the negative permittivity and permeability bandwidth in terms of the topological parameters of the structure. After that, in a third section, the topology with coated spheres is introduced. The theoretical model for this topology is constructed, and verified with CST simulations. Results for coated spheres are compared with results for nude spheres. It is proven that coating allows to considerably increase either the negative permeability or negative permittivity bandwidth. Note that in Sections 2 and 3, the main goal is to study separately the negative permittivity and negative permeability bands of the coated sphere structure, i.e., center frequency and bandwidth of these (possibly different) bands. The actual realization of a wide band NRI metamaterial is reported in the fourth and last section, where an array of wires is added, yielding a structure of both coated spheres and wires. The NRI bandwidth reached there is ca. 23%.

2. ARRAY OF NUDE SPHERES

Consider a structure consisting of a lattice of dielectric particles. If the radius of the particles is much smaller than the wavelength in the mixture, the mixture can be seen as a homogeneous material. Its effective properties can be obtained from the generalized Clausius-Mossotti relations [13] near the first two Mie resonance modes

$$\frac{\varepsilon_{eff} - \varepsilon_b}{\varepsilon_{eff} + 2\varepsilon_b} = \frac{N\alpha}{3} \tag{1}$$

$$\frac{\mu_{eff} - \mu_b}{\mu_{eff} + 2\mu_b} = \frac{N\beta}{3} \tag{2}$$

where, ε_{eff} and μ_{eff} are the effective permittivity and permeability of the matrix. ε_b and μ_b are the permittivity and permeability of the background host material. α and β are the electric and magnetic polarizability of the particles, N is the number of spheres per unit volume. α and β are related to the scattering coefficients a_1 and b_1 of the first lowest electric and magnetic dipole modes [14].

$$\alpha = \frac{6\pi j b_1}{k_0^3} \tag{3}$$

$$\beta = \frac{6\pi j a_1}{k_0^3} \tag{4}$$
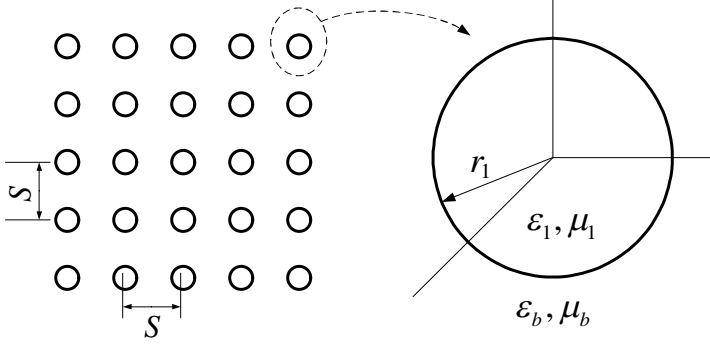
Figure 1. Array of spheres.

So we get

$$\varepsilon_{eff} = \varepsilon_b \frac{2(k_0 r)^3 + 6jf_v a_1}{2(k_0 r)^3 - 3jf_v a_1} \tag{5}$$

$$\mu_{eff} = \mu_b \frac{2(k_0 r)^3 + 6jf_v b_1}{2(k_0 r)^3 - 3jf_v b_1} \tag{6}$$

where $f_v = \frac{4}{3}\pi N r^3 = \frac{4\pi}{3}\left(\frac{r}{s}\right)^3$ is the volume fraction. r is the radius of the spheres and s is the distance between the sphere centers. For a certain array, once the scattering coefficients are calculated, the effective parameters are obtained from (5) and (6).

An array of "nude" spheres is shown in Fig. 1. The permittivity of the spheres is ε_1 and their radius is r_1. From Mie-scattering theory, the scattering coefficients are expressed as [27]

$$a_m = \frac{n_1 \psi_m(n_1 x_1)\psi_m'(x_1) - \psi_m(x_1)\psi_m'(n_1 x_1)}{n_1 \psi_m(n_1 x_1)\xi_m'(x_1) - \xi_m(x_1)\psi_m'(n_1 x_1)} \tag{7}$$

$$b_m = \frac{\psi_m(n_1 x_1)\psi_m'(x_1) - n_1\psi_m(x_1)\psi_m'(n_1 x_1)}{\psi_m(n_1 x_1)\xi_m'(x_1) - n_1\xi_m(x_1)\psi_m'(n_2 x_1)} \tag{8}$$

where $n_1 = \sqrt{\varepsilon_1 \mu_1}$, $x_1 = k_0 r_1$. $k_0 = \omega/c$ is the wave vector in vacuum. $\psi_m(z) = zj_m(z)$ and $\xi_m(z) = zh_m^{(1)}(z)$ are the m-th order Riccati-Bessel functions. The prime indicates a differentiation. Inserting (7) and (8) into (5) and (6), the Clausius-Mosotti model is obtained [13].

In this section, we will firstly prove that the Lewin model, established in 1947 [11], is identical to a simplified version of the Clausius-Mosotti model for the nude sphere. If $r_1 \ll \lambda/\sqrt{\varepsilon_b \mu_b}$, where λ is the wavelength in vacuum, the first two scattering coefficients can

be simplified [27]

$$a_1 = i\frac{2}{3}\left(k_0^2\varepsilon_b\mu_b\right)^{3/2}r_1^3\frac{\mu_b - \mu_p}{2\mu_b + \mu_p} \tag{9}$$

$$b_1 = i\frac{2}{3}\left(k_0^2\varepsilon_b\mu_b\right)^{3/2}r_1^3\frac{\varepsilon_b - \varepsilon_p}{2\varepsilon_b + \varepsilon_p} \tag{10}$$

$$\frac{\varepsilon_p}{\varepsilon_1} = \frac{\mu_p}{\mu_1} = \frac{2\left(\sin\theta - \theta\cos\theta\right)}{\left(\theta^2 - 1\right)\sin\theta + \theta\cos\theta} = F\left(\theta\right) \tag{11}$$

where $\theta = kr_1\sqrt{\varepsilon_1\mu_1}$, so the effective permittivity and permeability are easy to express as

$$\varepsilon_{\mathit{eff}} = \varepsilon_b\left(1 + 3f\middle/\left(\frac{\varepsilon_p + 2\varepsilon_1}{\varepsilon_p - \varepsilon_1} - f_v\right)\right) \tag{12}$$

$$\mu_{\mathit{eff}} = \mu_b\left(1 + 3f\middle/\left(\frac{\mu_p + \mu\varepsilon_1}{\mu_p - \mu_1} - f_v\right)\right) \tag{13}$$

These formulas are identical to the Maxwell-Garnett formulas obtained in a totally different way with the Lewin's model.

An example is calculated to compare the Lewin's model and the Clausius-Mossotti model. It is assumed that the background material and the spheres have the properties $\varepsilon_b = 1$, $\mu_b = 1$, $\varepsilon_1 = 150$ and $\mu_1 = 1$, respectively. The radius of the spheres is $r_1 = 5\,\mathrm{mm}$ and the distance between them is $s = 20\,\mathrm{mm}$. Fig. 2 shows the results. It can be seen that Lewin's model is very accurate. The two curves nearly coincide. The bands of negative permittivity and permeability appear alternately at the resonant frequencies. The lowest resonant frequency
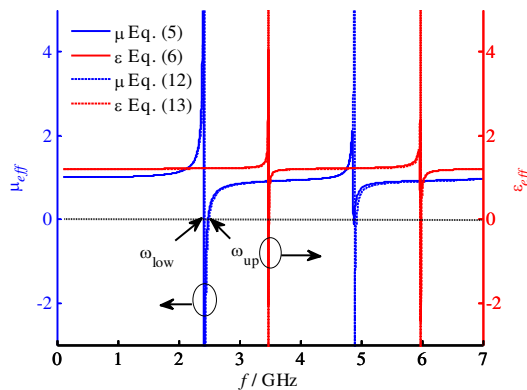
Figure 2. Effective parameters of an array of nude spheres ($s = 20\,\mathrm{mm}$, $r_1 = 5\,\mathrm{mm}$, $\varepsilon_1 = 150$).

corresponds to a negative permeability, showing a much wider band than the negative permittivity band displayed by the second resonant frequency.

Further in the paper the center frequencies and relative bandwidths for the resonances are defined as: $\omega_{center} = (\omega_{up} + \omega_{low})/2$ and $\omega_{RBW} = (\omega_{up} - \omega_{low})/2\omega_{center}$. ω_{up} and ω_{down} stand for the boundaries of the negative band as shown in Fig. 2. The following section discusses the relationships of ω_{center} and ω_{RBW} with ε_1, r_1 and s.
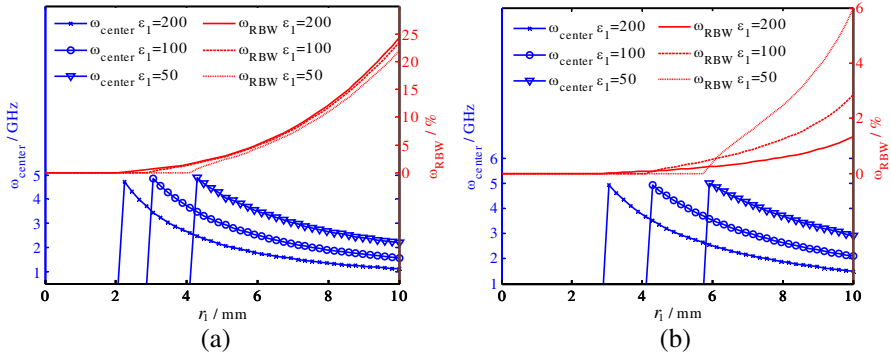
2.1. Change of ε_1 of the Spheres (Fig. 3)

Figure 3 exhibits the characteristics of the negative band with ε_1. When ε_1 is very small, there is no negative band. Above a certain value, the negative band appears. The center frequency of the resonance falls down as ε_1 increases, since the electric size of the spheres becomes larger.

Considering the bandwidth, the negative permeability and permittivity bands show different phenomena. For the negative permeability, the resonance becomes strong when ε_1 rises, so the band extends until it reaches a steady value. For the negative permittivity, the band increases sharply at first, also because the resonance becomes strong, but goes down immediately after it reaches its maximum. The reason is that the resonance, generating the negative component in the permittivity, cannot keep up with the average permittivity of the mixture, which is also increasing.
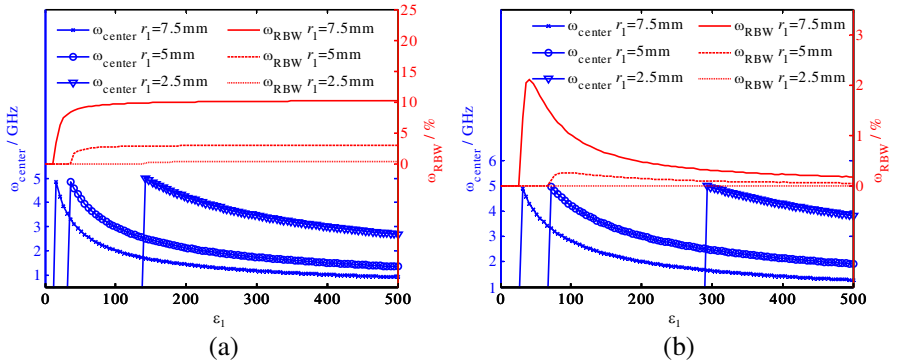
Figure 3. The change of the negative band with ε_1 ($s = 20\,\text{mm}$). (a) Effective permeability. (b) Effective permittivity.

Figure 4. The change of the negative band with r_1 ($s = 20\,\text{mm}$). (a) Effective permeability. (b) Effective permittivity.

2.2. Change of r_1 of the Spheres (Fig. 4)

In Fig. 4, ω_{center} goes down as r_1 increases, while ω_{RBW} grows caused by the coupling between the spheres. When r_1 is too small compared to s, the negative band will not appear. For different ε_1, the negative μ_{eff} band is almost identical, while the negative ε_{eff} band is very different. Note that the topologies with r_1 approaching 10 mm are not suitable in practice, since they correspond to cases where the spheres almost touch each other. In this case, also note that the strong coupling between the particles may induce a strange resonance, as fully described in [26]. A very narrow extra NRI band is obtained.

2.3. Change of s Between the Spheres (Fig. 5)

With changing the distance s, ω_{center} seems to keep its value. The center frequency is mainly caused by the structure of the particle itself, while the bandwidth is influenced by the embedding of the particle in an array configuration. Indeed, it can be seen that when s is too large, the resonance of this single particle cannot generate the negative aspect any more over the whole unit cell and the negative band disappears.

Generally speaking, the center frequency ω_{center} is mainly related to the size and permittivity of the spheres, while the bandwidth ω_{RBW} is related to the spacing in the array. Usually, foam with $\varepsilon_b = 1$ is chosen as the host medium, so only three parameters, s, r_1, and ε_1, can be adjusted in order to design the MMs for the nude spheres.
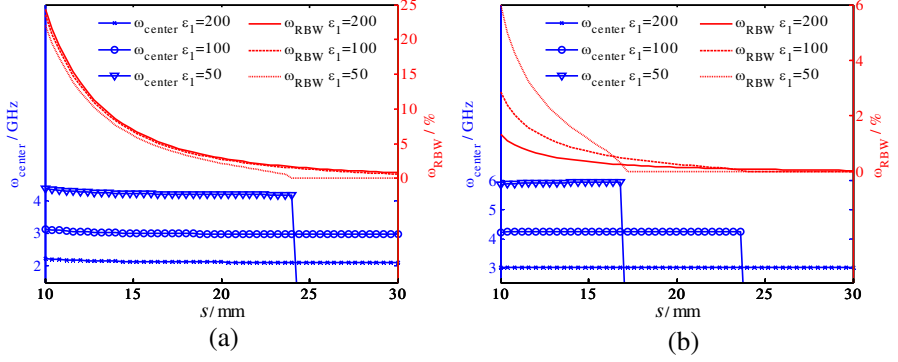
Figure 5. The change of the negative band with s ($r_1 = 5\,\mathrm{mm}$). (a) Effective permeability. (b) Effective permittivity.
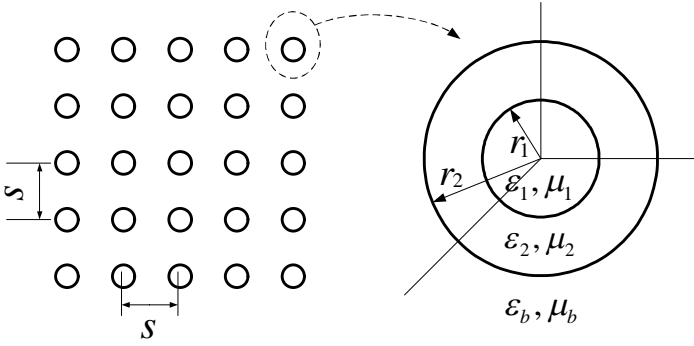
Figure 6. Array of coated spheres.

3. ARRAY OF COATED SPHERES

In this section an array of coated spheres, as shown in Fig. 6, is studied. There are five parameters in this topology: the two permittivities, the radii of the core and the coating, and the spacing in the array. We will show that if the five parameters are chosen properly, the bandwidth of the negative band is increased remarkably.

The core of the particle has the radius r_1 and permittivity ε_1 and the coating has an outer radius r_2 and permittivity ε_2. The scattering

coefficients of the coated spheres are [27]

$$a_m = \frac{\psi_m(x_2)[\psi_m'(n_2x_2) - A_m\chi_m'(n_2x_2)] - n_2\psi_m'(x_2)[\psi_m(n_2x_2) - A_m\chi_m(n_2x_2)]}{\xi_m(x_2)[\psi_m'(n_2x_2) - A_m\chi_m'(n_2x_2)] - n_2\xi_m'(x_2)[\psi_m(n_2x_2) - A_m\chi_m(n_2x_2)]} \quad (14)$$

$$b_m = \frac{n_2\psi_m(x_2)[\psi_m'(n_2x_2) - B_m\chi_m'(n_2x_2)] - \psi_m'(x_2)[\psi_m(n_2x_2) - B_m\chi_m(n_2x_2)]}{n_2\xi_m(x_2)[\psi_m'(n_2x_2) - B_m\chi_m'(n_2x_2)] - \xi_m'(x_2)[\psi_m(n_2x_2) - B_m\chi_m(n_2x_2)]} \quad (15)$$

$$A_m = \frac{n_2\psi_m(n_2x_1)\,\psi_m'(n_1x_1) - n_1\psi_m'(n_2x_1)\,\psi_m(n_1x_1)}{n_2\chi_m(n_2x_1)\,\psi_m'(n_1x_1) - n_1\chi_m'(n_2x_1)\,\psi_m(n_1x_1)} \quad (16)$$

$$B_m = \frac{n_2\psi_m(n_1x_1)\,\psi_m'(n_2x_1) - n_1\psi_m(n_2x_1)\,\psi_m'(n_1x_1)}{n_2\chi_m'(n_2x_1)\,\psi_m(n_1x_1) - n_1\psi_m'(n_1x_1)\,\chi_m(n_2x_1)} \quad (17)$$

where $n_1 = \sqrt{\varepsilon_1\mu_1}$, $n_2 = \sqrt{\varepsilon_2\mu_2}$, $x_1 = k_0r_1$, $x_2 = k_0r_2$. $\psi_m(z) = zj_m(z)$, $\xi_m(z) = zh_m^{(1)}(z)$ and $\chi_m(z) = -zy_m(z)$ are the m-th order Riccati-Bessel functions. The a_m and b_m are clearly different compared to the nude spheres. As for the nude spheres, the effective parameters of the coated spheres are obtained by inserting (14) and (15) into (5) and (6).

Note that in case that $r_1 \ll \lambda/\sqrt{\varepsilon_b\mu_b}$ and $r_2 \ll \lambda/\sqrt{\varepsilon_b\mu_b}$, a line of reasoning can be followed similar as in the case of a nude sphere to derive simplified formulas for the scattering coefficients. These can be used in (5) and (6) to yield a model similar as the Maxwell-Garnett model for the nude sphere. Full details can be found in [17]. See also [28] and [29], from which it can be seen that indeed the same results are obtained.

3.1. Change of r_1 of the Spheres (Fig. 7 and Fig. 8)

The outer radius of the coated spheres is kept at 5 mm, but the ratio of inter and outer radius (r_1/r_2) is changed. The distance s is kept at 20 mm. The core permittivity ε_1 is assumed 200, and the coated permittivity ε_2 is larger than ε_1 in Fig. 7 and smaller than ε_1 in Fig. 8. For $\varepsilon_2 > \varepsilon_1$, ω_{center} starts lower for both permeability and permittivity, compared with nude spheres. As the coating become thinner, ω_{center} grows gradually until we get the nude situation. But the bandwidth of permeability and permittivity varies differently. ω_{RBW} of μ_{eff} firstly goes up smoothly. After a maximum corresponding with a thin coating less than 1 mm, it goes down again. It is remarkable that the coated situation can give a larger ω_{RBW} than a single layer sphere with ε_2 or ε_1. This shows that coated spheres indeed have the capability to enlarge the bandwidth of negative μ_{eff}.

When the permittivity of the coating is lower than the core permittivity ($\varepsilon_2 < \varepsilon_1$), the situation is opposite. The ω_{center} becomes higher and the ω_{RBW} of μ_{eff} has a minimum value. Considering
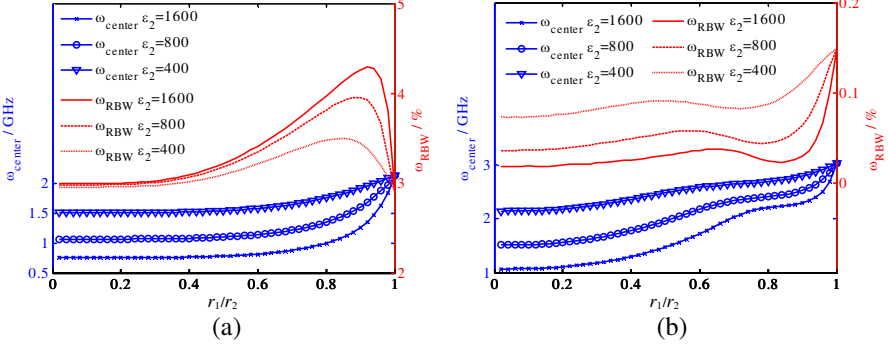
Figure 7. The change of negative band with r_1 ($s = 20\,\text{mm}$, $r_2 = 5\,\text{mm}$, $\varepsilon_1 = 200$, $\varepsilon_2 > \varepsilon_1$). (a) Effective permeability. (b) Effective permittivity.
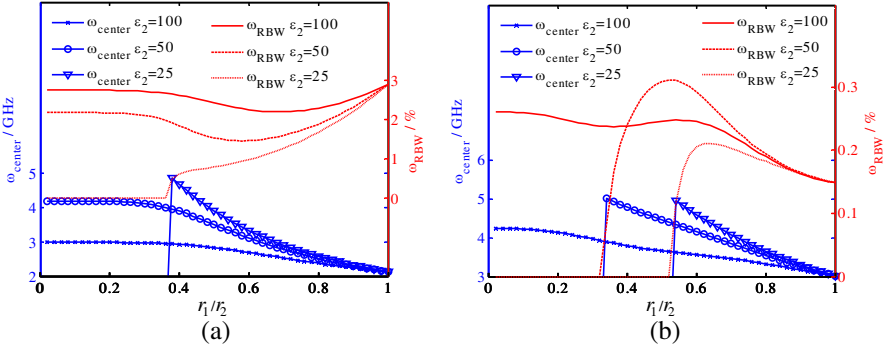
Figure 8. The change of negative band with r_1 ($s = 20\,\text{mm}$, $r_2 = 5\,\text{mm}$, $\varepsilon_1 = 200$, $\varepsilon_2 < \varepsilon_1$). (a) Effective permeability. (b) Effective permittivity.

the ω_{RBW} of ε_{eff}, the negative band is larger than for the nude sphere with the pure core permittivity ε_1. But it does not show a notable improvement compared to the nude sphere with the coating permittivity ε_2 (for example, $\varepsilon_2 = 100$, $\varepsilon_1 = 200$).

3.2. Change ε_2 of the Spheres (Fig. 7, Fig. 8 and Fig. 9)

In this section a different ε_2 is considered, while the core permittivity ε_1 remains 200. In Fig. 7, ε_2 is greater than ε_1. The higher ε_2 is responsible for the lower resonant frequency of both μ_{eff} and ε_{eff}. The bandwidth of μ_{eff} becomes larger as ε_2 grows. For a coating layer

with suitable thickness ($\varepsilon_2 = 1600$, $r_1/r_2 = 0.92$), the bandwidth reaches a maximum of 4.3%, nearly 50% above the original one of 2.9%. Unfortunately, the bandwidth of ε_{eff} is lower than the original.

In Fig. 8, ε_2 is less than ε_1. It can be seen in the figure that there is no negative band when ε_2 is too small and r_1 is too thin. With this kind of coating, ω_{center} of both μ_{eff} and ε_{eff} is higher. The variation of the bandwidth show opposite trends compared to Fig. 7.

In Fig. 9, r_1 is kept at 4 mm. Analyzed as a function of ε_2, ω_{RBW} of μ_{eff} first increases rapidly and then "saturates". ω_{RBW} of ε_{eff} first sharply grows and then gradually decreases to a very low value.
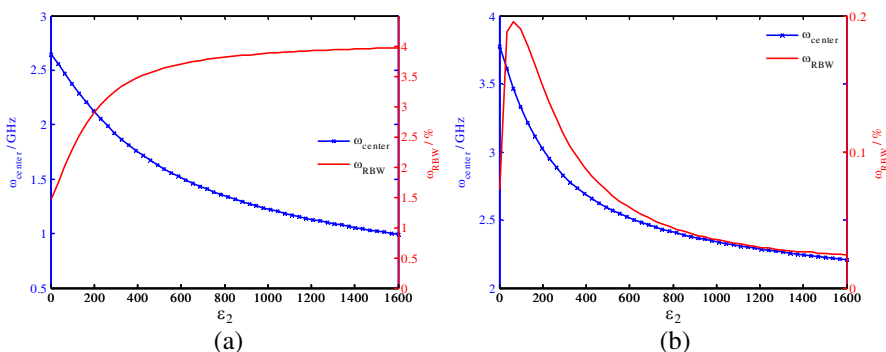
Figure 9. The change of negative band with ε_2 ($s = 20$ mm, $r_1 = 4$ mm, $r_2 = 5$ mm, $\varepsilon_1 = 200$). (a) Effective permeability. (b) Effective permittivity.
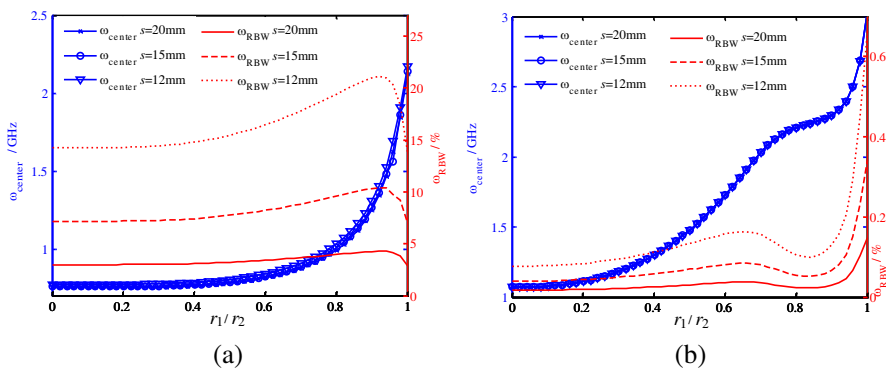
Figure 10. The change of the negative band with r_1 and s ($r_2 = 5$ mm, $\varepsilon_1 = 200$, $\varepsilon_2 = 1600$). (a) Effective permeability. (b) Effective permittivity.
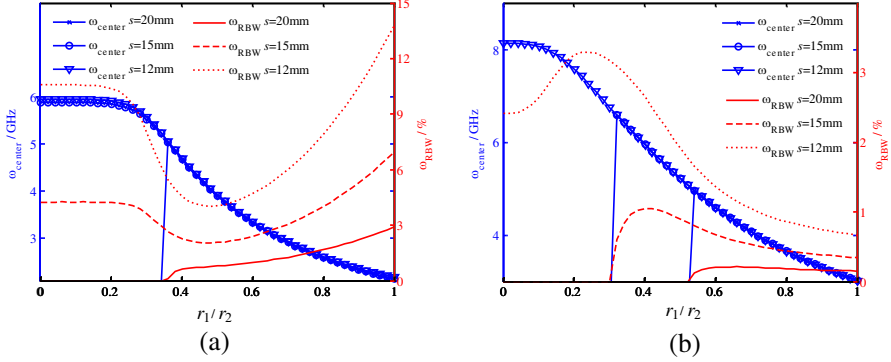
Figure 11. The change of the negative band with r_1 and s ($r_2 = 5\,\text{mm}$, $\varepsilon_1 = 200$, $\varepsilon_2 = 25$). (a) Effective permeability. (b) Effective permittivity.

3.3. Change s between the Spheres (Fig. 10 and Fig. 11)

In this section the distance s is changed, aiming at realizing a much wider negative parameter band, see Fig. 10 and Fig. 11. The distance between the coated spheres is chosen $12\,\text{mm}$, $15\,\text{mm}$, and $20\,\text{mm}$, respectively. It has to be emphasized that Fig. 10 and Fig. 11 are the key figures of the paper. They present the negative bands for a constant size (radius $5\,\text{mm}$) of the embedded particle. A higher coating permittivity ε_2 ($= 1600$) is chosen to increase the negative permeability band and a lower permittivity ε_2 ($= 25$) is chosen to increase the negative permittivity band. Like in the case of the nude sphere ω_{center} does not change with s, because ω_{center} is in practice only depending on the particle itself. However, ω_{RBW} grows continuously when the particles are put closer together since in that case the coupling between them is enhanced. It is clearly seen that a proper thickness of the coating can generate a much larger NRI bandwidth compared to cases where only a single permittivity is used. When only 25 is used as permittivity, there is no negative permittivity band for $s = 15\,\text{mm}$ and $20\,\text{mm}$ (the utmost left point in the Fig. 11(b)). When only 200 is used, the maximum negative permittivity BW is 0.7% for $s = 12\,\text{mm}$. For a coating of about $3.5\,\text{mm}$, the negative permittivity BW can be boosted up to 3.2%. Similarly, when we use a proper coating with permittivity 1600 (which is the highest practical value appearing in references), the negative permeability band can reach 22%, see Fig. 10(a). This is a really wide band for most applications.

4. VALIDATION AND APPLICATION

In order to verify the results of our model, several structures have been simulated with the frequency solver available in the commercial software CST Microwave Studio.

We mentioned before that the band of the negative permittivity is much narrower than the band of the negative permeability, see for example Fig. 3 and Fig. 5. Even the coated spheres can only provide a very narrow band with negative permittivity (Fig. 11(b)). That has a strong direct effect on the total bandwidth where a negative index n is obtained. But in microwave frequency bands, a negative permittivity can be easily obtained by an array of metallic wires ([30, 31]). If the radius of the wire is a and the spacing between them is s, the effective permittivity can be expressed as

$$\varepsilon_{eff} = 1 - \frac{1}{\frac{1}{2}\left(\frac{s}{2}\right)^2 \frac{\omega^2}{c^2} \ln\left(\frac{s}{2a}\right) + \frac{j\omega\varepsilon_0}{\sigma}\left(\frac{s}{2a}\right)^2} \tag{18}$$

where ω is the circular frequency and c the wave velocity in vacuum. In the topologies considered below, the dielectric spheres only provide the negative permeability at their first resonant frequency, and the array of metallic wires produces the negative permittivity.

Impedance z and refractive index n are widely used when characterizing electromagnetic materials. They can be related to ε and μ through $\varepsilon = n/z$ and $\mu = n^*z$. Usually, z and n are first retrieved from the simulation (in this work we use the technique of [32]), and then ε and μ are calculated.

This procedure is worked out as follows. In CST Microwave Studio, a waveguide with periodic boundaries is built to simulate infinite space, as shown in Fig. 12. A short section of vacuum waveguide is added at each end of the sample to ensure extinction of the higher order modes. We set one port at each side of this waveguide and obtain the S-matrix by simulation. This S-matrix is calculated back to the reference planes, also depicted in Fig. 12. This means that the results are actually obtained with respect to the reference planes, which are set at a unit cell boundary.

The number of unit cells actually simulated is based on the following line of reasoning. Since the periodic boundaries ensure periodicity in the transversal directions, transversally we can take one unit cell only. We have simulated different lengths of the 1D metamaterial sample. The result is that the retrieved values for permittivity and permeability are almost independent of the number of unit cells along the length, except for the artificial resonances due to the extraction procedure itself, as discussed in [33]. This is illustrated
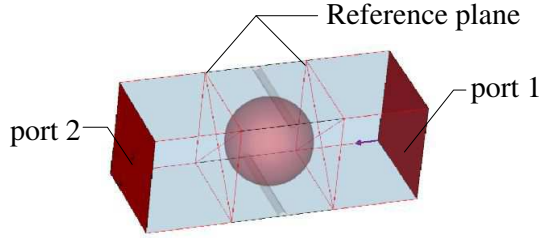
Figure 12. The topology of the CST model.
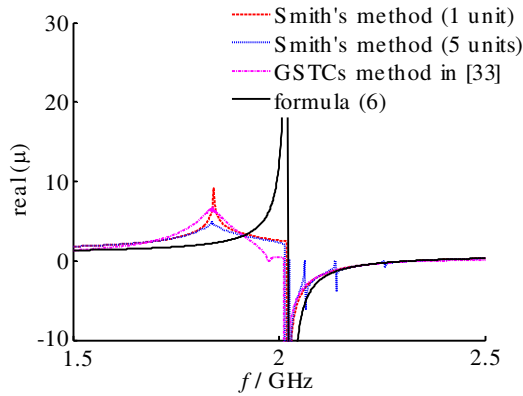
Figure 13. Comparison of different methods ($s = 12\,\mathrm{mm}$, $r_1 = 5\,\mathrm{mm}$, $\varepsilon_1 = 200$, $a = 0.5\,\mathrm{mm}$).

in Fig. 13. This means that using a single unit cell already provides accurate results.

In [35] it is stated that the problem of the boundary effects can be solved by using the original extraction technique in combination with a proper choice of the reference planes. However, in the same paper it is mentioned: "... to eventually conclude empirically that the first effective boundary of a symmetric one-dimensional metamaterial coincides with the first unit-cell boundary and the second effective boundary coincides with the last unit-cell boundary". This confirms that our choice of the reference planes is correct. If necessary, the technique of [33, 34] can be used to remove the remaining small surface effects. However, this will not change the main conclusions of this paper. This is illustrated in Fig. 13, where the method used in this paper (Smith's method, 1 unit) is compared to a case where multiple unit cells are considered (Smith's method, 5 units), and with the

method of [33]. As can be seen, the three methods almost completely coincide in the negative permeability region.

The S parameters are related to n and z by (see [32])

$$S_{11} = \frac{\Gamma\left(1 - e^{j2nk_0d}\right)}{1 - \Gamma^2 e^{j2nk_0d}} \tag{19}$$

$$S_{21} = \frac{\left(1 - \Gamma^2\right) e^{jnk_0d}}{1 - \Gamma^2 e^{j2nk_0d}} \tag{20}$$

with $k_0 = \frac{2\pi}{\lambda_0} = \frac{2\pi f}{c}$ and $\Gamma = \frac{z-1}{z+1}$. d is the length of the waveguide. This can be easily transformed into

$$z = \pm\sqrt{\frac{(1 + S_{11})^2 - S_{21}^2}{(1 - S_{11})^2 - S_{21}^2}} \tag{21}$$

$$n = \pm\frac{1}{k_0d}\cos\left[\frac{1}{2S_{21}}\left(1 - S_{11}^2 + S_{21}^2\right)\right] + \frac{2\pi m}{k_0d} \tag{22}$$

Pay attention, for passive materials, Real(z) and Imag(n) must be greater than zero. m is an integer related to the branch of index Real(n). For a thin thickness sample, m can be equaled to zero, while under other conditions, m has to be obtained from the continuity of n. More details on this retrieval method can be found in [35, 36].

4.1. Nude Spheres

In the topological model, the waveguide contains one unit element. Fig. 14 shows all corresponding results. Figs. 14(a) and (b) display the S parameters obtained by CST in three situations, only metallic wires, only nude spheres, and using them together. Figs. 14(c) and (d) reveal the parameters retrieved by using (21) and (22), compared with our model (using (6) and (18)). The metallic wires show a wide stop band for the whole simulation frequency range caused by the negative permittivity, while the configuration with nude spheres has an obvious stop band around its first resonant frequency 2.171 GHz, corresponding to the negative permeability. A combination of metallic wires and dielectric spheres can provide double negative parameters, so a pass band appears as expected. This pass band corresponds to a NRI bandwidth of 14.1%. This cannot be improved significantly by increasing the permittivity of the spheres, as shown by the permeability results in Fig. 3(a). On top, we simulated the NRI bandwidth for a structure with wires and for $\varepsilon_1 = 1600$. The result is only 13.8%.

The agreement between the permeability obtained from the CST simulation and from our model is excellent for the array of nude spheres. However, the resonant frequency shifts 0.01 GHz towards
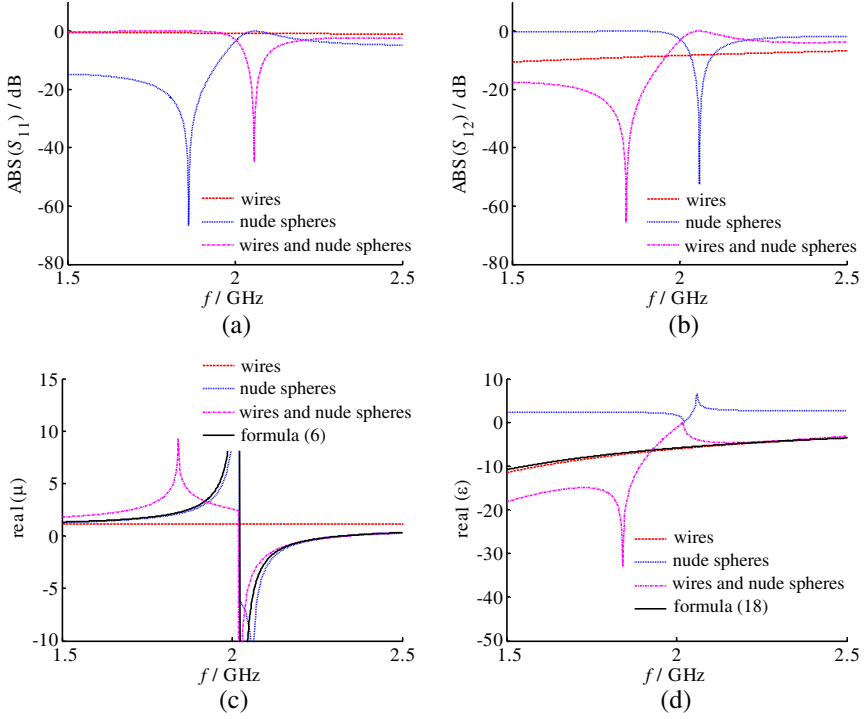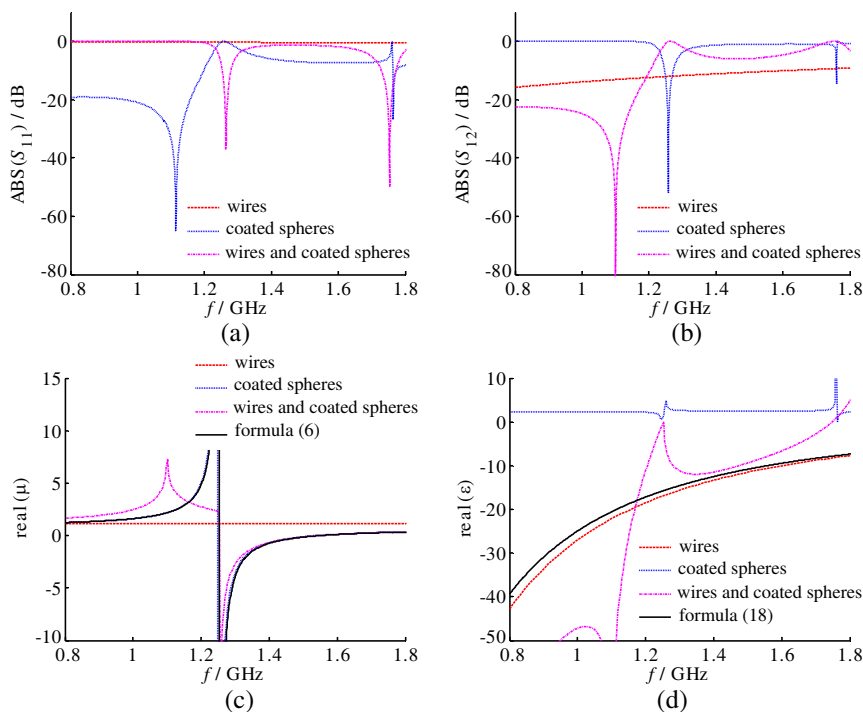
Figure 14. Topology of nude spheres ($s = 12$ mm, $r_1 = 5$ mm, $\varepsilon_1 = 200$, $a = 0.5$ mm). (a) S_{11} from CST. (b) S_{12} from CST. (c) Permeability. (d) Permittivity.

higher frequencies for the combination of metallic wires and nude spheres. This means that the metallic wires can influence the permeability a little bit.

The permittivity retrieved for the combination of metallic wires and nude spheres shows little difference with the results obtained from our model. For the CST simulation the permittivity is a little bit perturbed at the first magnetic resonance. This is not obtained from our model. However, this difference is little compared with the much larger influence of the metallic wires.

4.2. Coated Spheres

Also for the coated spheres, our formulas and the CST results agree well, as shown in Fig. 15. This proves the correctness of our model for the topology of coated spheres. Little difference still appears for the
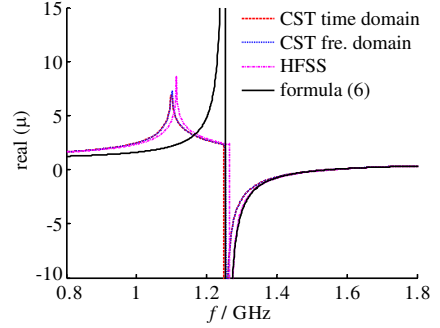
Figure 15. Topology of coated spheres ($s = 12\,\text{mm}$, $r_1 = 5\,\text{mm}$, $r_2 = 4.6\,\text{mm}$, $\varepsilon_1 = 200$, $\varepsilon_2 = 1600$, $a = 0.5\,\text{mm}$). (a) S_{11} from CST. (b) S_{12} from CST. (c) Permeability. (d) Permittivity.

structure mixing the metallic wires and spheres together, as mentioned for the nude spheres. It is clearly shown that the new technique allows to increase the NRI bandwidth. It is now 23% around a frequency of 1.34 GHz, which is an obvious improvement of 64% compared to the nude spheres of the last section ($\omega_{RBW} = 14\%$). Moreover, if we put the spheres more densely together, the relative band could even be further increased by using the mutual coupling, as shown in Fig. 5.

In Fig. 16, the amplitude of the electric displacement vector $\varepsilon\mathbf{E}$ on the center line of the waveguide at resonance is shown for three different cases: nudes spheres for $\varepsilon = 200$ and for $\varepsilon = 1600$, and coated spheres. No wires are present. The physical parameters of the spheres are the same as in Fig. 14 and Fig. 15. It is clearly seen that in the case of the coated spheres, inside the coating this vector (and thus the polarization current) is much larger than within the core spheres. This explains the possible strong effect on the scattering of the incident field, which in its turn explains the effect on the bandwidth, see (6).
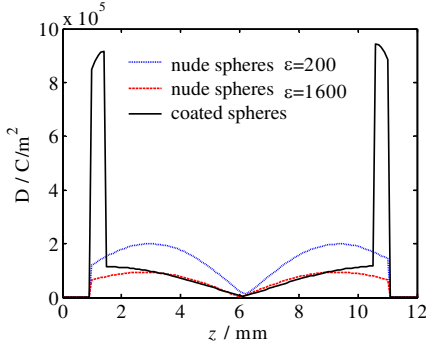
Figure 16. Comparison of the electric displacement vector within the spheres. Wires are not present and the physical parameters of these spheres are the same as in Fig. 14 and Fig. 15.

Figure 17. Comparison of different solvers for the topology of wires and coated spheres ($s = 12\,\text{mm}$, $r_1 = 5\,\text{mm}$, $r_2 = 4.6\,\text{mm}$, $\varepsilon_1 = 200$, $\varepsilon_2 = 1600$, $a = 0.5\,\text{mm}$).

In order to verify the results above-mentioned, based on the recommendation given in [37], the results of the frequency solver within CST are compared with the time-domain solver within CST and with HFSS. The results are given in Fig. 17. They indicate that the three different solvers agree extremely well. The CST time domain solver practically coincides with the CST frequency domain solver. The HFSS result shows a frequency shift of only 10 MHz (0.8%).

In order to assess the effect of realistic losses, the topology was also analyzed for $\varepsilon_1 = 200(1\text{-}j0.001)$, $\varepsilon_2 = 1600(1\text{-}j0.003)$, and $\sigma = 5.8 \times 10^7\,\text{S}$ for the metallic wires, respectively. The CST results yield an attenuation constant (defined as in [17]) of $\alpha = 1.12\,\text{dB}/\lambda$ at 1.35 GHz. This is a really low value very competitive with the values found in the overview Table 1 in [17].

Finally, in Table 1 we compare several kinds of NRI metamaterials described in literature. It can be clearly seen that the topology with coated spheres and wires has the second highest bandwidth of all the structures. The metallic crosses structure of [38] yields the widest band. It can be expected however that this structure is extremely sensitive to small deviations in the gap distances between the crosses, an issue not considered in [38]. The bandwidth in the last column is defined as the bandwidth where the real part of both permittivity and permeability are negative simultaneously.

Nude sphere metamaterials have been fabricated and verified in a few experiments [18–20]. The practical realization of coated spheres

Table 1. Comparison of several kinds of NRI metamaterials.

Ref.	Technology	Center Freq. [GHz]	NRI BW [%]
[2]	SRRs and wires	10.5	9
[5]	Ω-like metallic patterns	12.6	9.5
[7]	U-like metallic patterns	85×10^3	5.9
[38]	Metallic Crosses	11.5	56.7
[12]	Dielectric spheres	67.1	0.3
[13]	Dielectric spheres	10.1	1
[19]	Dielectric cubes and wires	8.6	3.7
[20]	Dielectric spheres and wires	6	11.7
[21]	Dielectric rods	10.8	3.7
[16]	Degenerate dielectric spheres	16.5	6
[15]	Micron-scale coated spheres	3.6×10^3	9.8
This paper	Coated dielectric spheres and wires	1.34	**23**

however is a huge challenge for researchers active in this field. One of the main reasons is that in the microwave frequency band, the high permittivity dielectrics involved are usually very fragile and extremely difficult to process mechanically. In the terahertz and optical frequency bands, it may be feasible to realize coated structures by using thin film technology.

5. CONCLUSION

In this paper, a specific case of a dielectric metamaterial is discussed. It involves spheres that are coated in order to extend the NRI bandwidth. By using suitable coating materials with optimal permittivity and thickness, the NRI bandwidth can be increased 60% compared with nude spheres with no coating. In order to obtain these results, an upgraded theoretical model is used and compared with general purpose commercial software. The agreement is excellent. The theoretical model provides an intuitive link between the physical size and the electromagnetic parameters, which can be used to design this kind of all-dielectric MMs.

REFERENCES

1. Veselago, V. G., "The electrodynamics of substances with simultaneously negative values of ε and μ," *Soviet Physics Uspekhi*, Vol. 10, 509–514, 1968.

2. Shelby, R. A., D. R. Smith, and S. Schultz, "Experimental verification of a negative index of refraction," *Science*, Vol. 292, 77–79, Apr. 2001.

3. Pendry, J. B., A. J. Holden, D. J. Robbins, and W. J. Stewart, "Magnetism from conductors and enhanced nonlinear phenomena," *IEEE Transactions on Microwave Theory and Techniques*, Vol. 47, 2075–2084, Nov. 1999.

4. Enkrich, C., M. Wegener, S. Linden, S. Burger, L. Zschiedrich, F. Schmidt, J. F. Zhou, T. Koschny, and C. M. Soukoulis, "Magnetic metamaterials at telecommunication and visible frequencies," *Phys. Rev. Lett.*, Vol. 95, 203901, 2005.

5. Huangfu, J., L. Ran, H. Chen, X. Zhang, K. Chen, T. M. Grzegorczyk, and J. A. Kong, "Experimental confirmation of negative refractive index of a metamaterial composed of Ω-like metallic patterns," *Appl. Phys. Lett.*, Vol. 84, 1537–1539, 2004.

6. Chen, H., L. Ran, J. Huangfu, X. M. Zhang, K. Chen, T. M. Grzegorczyk, and J. A. Kong, "Magnetic properties of S-shaped split-ring resonators," *Progress In Electromagnetics Research*, Vol. 51, 231–247, 2005.

7. Linden, S., C. Enkrich, M. Wegener, J. Zhou, T. Koschny, and C. M. Soukoulis, "Magnetic response of metamaterials at 100 terahertz," *Science*, Vol. 306, 1351–1353, Nov. 2004.

8. Bilotti, F., A. Toscano, and L. Vegni, "Design of spiral and multiple split-ring resonators for the realization of miniaturized metamaterial samples," *IEEE Transactions on Antennas and Propagation*, Vol. 55, 2258–2267, Aug. 2007.

9. Gans, R. and H. Happel, "Zur optik kolloidaler metallÄosungen," *Ann. Physik*, 277–300, 4th Folge, Bd. 29, 1909.

10. Holloway, C. L., E. F. Kuester, J. Baker-Jarvis, and P. Kabos, "A double negative (DNG) composite medium composed of magnetodielectric spherical particles embedded in a matrix," *IEEE Transactions on Antennas and Propagation*, Vol. 51, 2596–2603, Oct. 2003.

11. Lewin, L., "The electrical constants of a material loaded with spherical particles," *Electrical Engineers — Part III: Radio and Communication Engineering*, Vol. 94, 65–68, Jan. 1947.

12. Vendik, O. G. and M. S. Gashinova, "Artificial double negative (DNG) media composed by two different dielectric sphere lattices embedded in a dielectric matrix," *34th European Microwave Conference 2004*, Vol. 3, 1209–1212, Oct. 2004.

13. Jylhä, L., I. Kolmakov, S. Maslovski, and S. Tretyakov, "Modeling of isotropic backward-wave materials composed of resonant spheres," *J. Appl. Phys.*, Vol. 99, 043102, 2006.

14. Sihvola, A., *Electromagnetic Mixing Formulas and Applications*, IEE Electromagnetic Waves Series, Vol. 47, The Institution of Electrical Engineers, Stevenage, Herts, UK, 1999.

15. Wheeler, M. S., J. S. Aitchison, and M. Mojahedi, "Coated nonmagnetic spheres with a negative index of refraction at infrared frequencies," *Phys. Rev. B*, Vol. 73, 045105, 2006.

16. Basilio, L. I., L. K. Warne, W. L. Langston, W. A. Johnson, and M. B. Sinclair, "Microwave-frequency, negative-index metamaterial designs based on degenerate dielectric resonators," *IEEE Antennas and Wireless Propagation Letters*, Vol. 11, 113–116, Jan. 2012.

17. Kuester, E. F., N. Memic, S. Shen, A. Scher, S. Kim, K. Kumley, and H. Loui, "A negative refractive index metamaterial based on a cubic array of layered nonmagnetic spherical particles," *Progress In Electromagnetics Research B*, Vol. 33, 175–202, 2011.

18. Peng, L., L. Ran, H. Chen, H. Zhang, J. A. Kong, and T. M. Grzegorczyk, "Experimental observation of left-handed behavior in an array of standard dielectric resonators," *Phys. Rev. Lett.*, Vol. 98, 157403, 2007.

19. Zhao, Q., L. Kang, B. Du, H. Zhao, Q. Xie, X. Huang, B. Li, J. Zhou, and L. Li, "Experimental demonstration of isotropic negative permeability in a three-dimensional dielectric composite," *Phys. Rev. Lett.*, Vol. 101, 027402, 2008.

20. Cai, X., R. Zhu, and G. Hu, "Experimental study for metamaterials based on dielectric resonators and wire frame," *Metamaterials*, Vol. 2, 220–226, Dec. 2008.

21. Lepetit, T., É. Akmansoy, and J.-P. Ganne, "Experimental measurement of negative index in an all-dielectric metamaterial," *Appl. Phys. Lett.*, Vol. 95, 121101, 2009.

22. Liu, L., J. Sun, X. Fu, J. Zhou, Q. Zhao, B. Fu, J. Liao, and D. Lippens, "Artificial magnetic properties of dielectric metamaterials in terms of effective circuit model," *Progress In Electromagnetics Research*, Vol. 16, 159–170, 2011.

23. Yannopapas, V. and A. Moroz, "Negative refractive index

metamaterials from inherently non-magnetic materials for deep infrared to terahertz frequency ranges," *Journal of Physics: Condensed Matter*, Vol. 17, 3717, 2005.

24. Garcia-Etxarri, A., R. Gomez-Medina, L. S. Froufe-Perez, C. Lopez, L. Chantada, F. Scheffold, J. Aizpurua, M. Nieto-Vesperinas, and J. J. Saenz, "Strong magnetic response of submicron Silicon particles in the infrared," *Optics Express*, Vol. 19, 4815, Mar. 2011.

25. Ahmadi, A. and H. Mosallaei, "All-dielectric metamaterial: Double negative behavior and bandwidth-loss improvement," *Antennas and Propagation Society International Symposium*, 5527–5530, Jun. 2007.

26. Vendik, I. B., M. A. Odit, and D. S. Kozlov, "3D isotropic metamaterial based on a regular array of resonant dielectric spherical inclusions," *Metamaterials*, Vol. 3, 140–147, 2009.

27. Bohren, C. F. and D. R. Huffman, *Absorption and Scattering of Light by Small Particles*, Wiley, University of California, Berkeley, 1983

28. Tserkezis, C., C. Gantzounis, and N. Stefanou, "Collective plasmonic modes in ordered assemblies of metallic nanoshells," *Journal of Physics: Condensed Matter*, Vol. 20, 075232, 2008.

29. Li, J., G. Sun, and C. T. Chan, "Optical properties of photonic crystals composed of metal-coated spheres," *Phys. Rev. B*, Vol. 73, 075117, 2006.

30. Pendry, J. B., A. J. Holden, W. J. Stewart, and I. Youngs, "Extremely low frequency plasmons in metallic mesostructures," *Phys. Rev. Lett.*, Vol. 76, 4773–4776, 1996.

31. Pendry, J. B., A. J. Holden, D. J. Robbins, and W. J. Stewart, "Low frequency plasmons in thin-wire structures," *Journal of Physics: Condensed Matter*, Vol. 10, 1998, 4785.

32. Smith, D. R., S. Schultz, P. Markoš, and C. M. Soukoulis, "Determination of effective permittivity and permeability of metamaterials from reflection and transmission coefficients," *Phys. Rev. B*, 65, 195104, 2002.

33. Kim, S., E. F. Kuester, C. L. Holloway, A. D. Scher, and J. Baker-Jarvis, "Boundary effects on the determination of metamaterial parameters from normal incidence reflection and transmission measurements," *IEEE Transactions on Antennas and Propagation*, Vol. 59, 2226, Jun. 2011.

34. Kim, S., E. F. Kuester, C. L. Holloway, A. D. Scher, and J. Baker-Jarvis, "Effective material property extraction of a metamaterial

by taking boundary effects into account at TE/TM polarized incidence," *Progress In Electromagnetics Research B*, Vol. 36, 1–33, 2012.

35. Chen, X., T. M. Grzegorczyk, B. Wu, J. Pacheco, and J. A. Kong, "Robust method to retrieve the constitutive effective parameters of metamaterials," *Phys. Rev. E*, Vol. 70, 016608, 2004.

36. Smith, D. R., D. C. Vier, T. Koschny, and C. M. Soukoulis, "Electromagnetic parameter retrieval from inhomogeneous metamaterials," *Phys. Rev. E*, Vol. 71, 036617, 2005.

37. Vasylchenko, A., Y. Schols, W. De Raedt, and G. A. E. Vandenbosch, "Quality assessment of computational techniques and software tools for planar antenna analysis," *IEEE Antennas Propagat. Magazine*, Vol. 51, No. 1, 23–38, Feb. 2009.

38. He, X., Y. Wang, J. Mei, T. Gui, and J. Yin, "Three-dimensional surface current loops in broadband responsive negative refractive metamaterial with isotropy," *Chinese Physics B*, Vol. 21, 044101, 2012.